Karbala International Journal of Modern Science

Volume 8 | Issue 2 Article 2

Heterogeneous catalytic degradation of dye by Fenton-like oxidation over a continuous system based on Box–Behnken design and traditional batch experiments

Imad M. Luaibi
Al-Khwarizmi College of Engineering, University of Baghdad, Baghdad, Iraq, emad.iq84@gmail.com

Mohammed A. Atiya
Al-Khwarizmi College of Engineering, University of Baghdad, Baghdad, Iraq

Ahmed K. Hassan
Department of Treatment of Haz-Mat, Environment and Water Directorate, Ministry of Science and Technology, Baghdad, Iraq

Zainab A. Mahmoud
Al-Khwarizmi College of Engineering, University of Baghdad, Baghdad, Iraq

Recommended Citation

Luaibi, Imad M.; Atiya, Mohammed A.; Hassan, Ahmed K.; and Mahmoud, Zainab A. (2022) "Heterogeneous catalytic degradation of dye by Fenton-like oxidation over a continuous system based on Box–Behnken design and traditional batch experiments," *Karbala International Journal of Modern Science*: Vol. 8 : Iss. 2 , Article 2.
Available at: https://doi.org/10.33640/2405-609X.3217

Heterogeneous catalytic degradation of dye by Fenton-like oxidation over a continuous system based on Box–Behnken design and traditional batch experiments

Abstract

In this study, iron was coupled with copper to form a bimetallic compound through a biosynthetic method, which was then used as a catalyst in the Fenton-like processes for removing direct Blue 15 dye (DB15) from aqueous solution. Characterization techniques were applied on the resultant nanoparticles such as SEM, BET, EDAX, FT-IR, XRD, and zeta potential. Specifically, the rounded and shaped as spherical nanoparticles were found for green synthesized iron/copper nanoparticles (G-Fe/Cu NPs) with the size ranging from 32-59 nm, and the surface area was 4.452 m2/g. The effect of different experimental factors was studied in both batch and continuous experiments. These factors were H2O2 concentration, G-Fe/Cu-NPs amount, pH, initial DB15 concentration, and temperature in the batch system. The batch results showed 98% of 100 mg/L of DB15 was degraded with optimum H2O2 concentration, G-Fe/Cu-NPs dose, pH, and temperature 3.52 mmol/L, 0.7 g/L, 3, and 50°C respectively. For the continuous mode, the influences of initial DB15 concentration, feed flow rate, G-Fe/Cu-NPs depth were investigated using an optimized experimental Box-Behnken design, while the conditions of pH and H2O2 concentration were based on the best value found in the batch experiments. The model optimization was set the parameters at 2.134 ml/min flow rate, 26.16 mg/L initial dye concentration, and 1.42 cm catalyst depth. All the parameters of the breakthrough curve were also studied in this study including break time, saturation time, length of mass transfer zone, the volume of bed, and volume effluent.

Keywords

Fenton-like, Bimetallic nanoparticles, Direct blue 15 dye, Fixed-bed column, Breakthrough curve.

RESEARCH PAPER

Heterogeneous Catalytic Degradation of Dye by Fenton-like Oxidation Over a Continuous System Based on Box−Behnken Design and Traditional Batch Experiments☆

Imad M. Luaibi [a,*], Mohammed A. Atiya [a], Ahmed K. Hassan [b], Zainab A. Mahmoud [a]

[a] Al-Khwarizmi College of Engineering, University of Baghdad, Baghdad, Iraq
[b] Environment and Water Directorate, Ministry of Science and Technology, Baghdad, Iraq

Abstract

In this study, iron was coupled with copper to form a bimetallic compound through a biosynthetic method, which was then used as a catalyst in the Fenton-like processes for removing direct Blue 15 dye (DB15) from aqueous solution. Characterization techniques were applied on the resultant nanoparticles such as SEM, BET, EDAX, FT-IR, XRD, and zeta potential. Specifically, the rounded and shaped as spherical nanoparticles were found for green synthesized iron/copper nanoparticles (G-Fe/Cu NPs) with the size ranging from 32 to 59 nm, and the surface area was 4.452 m^2/g. The effect of different experimental factors was studied in both batch and continuous experiments. These factors were H_2O_2 concentration, G-Fe/Cu-NPs amount, pH, initial DB15 concentration, and temperature in the batch system. The batch results showed 98% of 100 mg/L of DB15 was degraded with optimum H_2O_2 concentration, G-Fe/Cu-NPs dose, pH, and temperature 3.52 mmol/L, 0.7 g/L, 3, and 50 °C respectively. For the continuous mode, the influences of initial DB15 concentration, feed flow rate, G-Fe/Cu-NPs depth were investigated using an optimized experimental Box-Behnken design, while the conditions of pH and H_2O_2 concentration were based on the best value found in the batch experiments. The model optimization was set the parameters at 2.134 ml/min flow rate, 26.16 mg/L initial dye concentration, and 1.42 cm catalyst depth. All the parameters of the breakthrough curve were also studied in this study including break time, saturation time, length of mass transfer zone, the volume of bed, and volume effluent.

Keywords: Fenton-like, Bimetallic nanoparticles, Direct blue 15 dye, Fixed-bed column, Breakthrough curve

1. Introduction

Nowadays, water management is one of the biggest challenges facing the world, especially with the increasing population and developing industries [1]. Polluted water sources with various contaminants like dyes have raised environmental and health concerns. Generally, various textile production activities are contributed to release of one-fifth of the world's dyes production to the water sources causing negative effects on human health and the aquatic ecosystem [2,3].

Therefore, numerous technologies have been developed to remove or degrade the dyes from wastewater such as adsorption [4], electrocoagulation [5], phytoremediation [6] advanced oxidation processes (AOPs) [7], membrane separation [8], and coagulation [9,10]. Some of these technologies have their drawbacks, where the membrane method is expensive, forms sludge, and rapid membrane fouling. The disadvantages of

☆ Special description of the title. (dispensable).

Received 2 September 2021; revised 23 January 2022; accepted 27 January 2022.
Available online 1 May 2022

* Corresponding author at:
E-mail addresses: emad.iq84@gmail.com (I.M. Luaibi), mohatiya1965@gmail.com (M.A. Atiya), ahmedkhh71@yahoo.com (A.K. Hassan), zainab.amahmoud@gmail.com (Z.A. Mahmoud).

https://doi.org/10.33640/2405-609X.3217

coagulation technology can be summarized by high concentrated sludge production and not being effective for azo dye. Also, phytoremediation is not efficient to be adopted due to a long time of water and wastewater treatment. Moreover, resins that used in the adsorption method are considered very expensive leading to an increase in the operational cost of this system [11,12]. Despite pH-dependent as well as the side-product generation in the AOPs, they are characterized by fully destroying the risky and complex materials and making them very suitable for dyes removal [7,11,13]. However, the eco-friendly method of AOPs is the heterogeneous Fenton oxidation (also named Fenton-like) which is working based on producing high reactive ·OH radicals through the reaction between catalysts like Fe^{+3}, Fe^{+2}/Fe^{+3}, or Cu^{+2} and hydrogen peroxide. These radicals can initiate a fast oxidation process of organic contaminants, thereby degrading these pollutants [14,15].

Among many catalysts that have been used in the Fenton-like processes, iron nanoparticles are very high active to remove these types of pollutants [16]. Additionally, iron-based is a promising technique used as a Fenton-like catalyst by adding a second catalyst such as Cu, Pt, Pd, Ni, Mn to the iron [17,18]. The mutual effect of two metals improves the catalytic activity of nanoparticles over the use of just one metal (monometallic); therefore, bimetallic nanoparticles have become of great interest to researchers [19,20]. Bimetallic nanoparticles can be synthesized using the green biological technique which is considered an alternative technique to chemical and physical synthesis. This technique uses leaves extract of plants with economic feasibility and reliability and no complexity of synthetic [21,22].

In the last few years, the batch reactors of Fenton-like reactions have been widely studied for the water treatments field. However, this type of system is not environmentally friendly due to the increase in the discharge of pollutants by various factories. Therefore, the attention turned to the systems that can treat these pollutants continuously without affecting the environment [1]. In the continuous system, the interaction between catalyst and solute is already carried out by numerous systems such as fixed-bed and fluidized-bed, etc. However, a fixed bed is a more beneficial and practical method to treat different synthetic and real water pollutants. It is a simple and cost-effective technique compared to fluidized beds as well as treating higher amounts of pollutants than the batch system [23]. The high performance of fixed-bed is due to cyclic removal which is related to the gradient in concentration thereby forming a driving force for sorption, where these forces enhance the adsorbent capacity by efficient usage [24]. The removal process in continuous flow mode using fixed-bed depends on continuous mass transfer occurs between two phases (the mobile phase which represents the contaminated solution and the solid phase of nanoparticles in the column bed). The solute concentration in both phases is a function of contact time and the height of the mass transfer zone (MTZ).

Recently, statistical experiments using software design were extensively applied instead of the classical methods to minimize the number of experiments required to optimize the process response at a high level of confidence, thereby saving costs and time [25]. Moreover, these statistical theories are also applied to identify a mathematical model representing the process variables, with data analysis, signification, and optimization. Therefore, it was adopted by the Taguchi method, full factorial design, and response surface methodology (RSM). Among these approaches, RSM is stand out as the highly utilized method to optimize parameters of the statistical experiments [26]. The RSM is a rotatable design that successive in revealing the effect of the interaction among the independent variables and process response from experimental data formed with 3D surface and contour plots associated with the regression model. Additionally, RSM branches into two major ways which are Box-Behnken design (BBD) and central composite design (CCD).

This study aims to prepare iron/copper nanoparticles by a green method using the extract from the ficus plant. These nanoparticles can be applied as a heterogeneous catalyst in the complete Fenton-like experiments using batch and fixed-bed for removing DB15 dye from wastewater. Finally, the dye degradation processes in the fixed-bed were optimized with the assistance of the statistical analysis design of experiments (BBD).

2. Material and methods

2.1. Chemical and reagents

The purity of all chemicals utilized in our experiments was very high (99.9%). Ficus leaves were collected from the University of Baghdad, Iraq. The DB15 was purchased from Central Drug House (BDH) Company with all properties shown in Table 1. Ferrous sulfate heptahydrate ($FeSO_4.7H_2O$), the hydrogen peroxide (50% w/w) and sodium sulfite were purchased from BDH company. Copper

Table 1. Physical and chemical properties of direct blue 15 (DB15) dye.

Properties of (DB15)	
Molecular structure	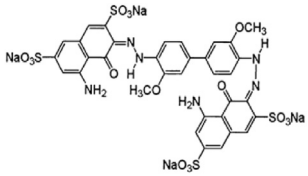
Molecular formula	$C_{34}H_{24}N_6Na_4O_{16}S_4$
Molecular weight (g/mole)	992.8
Color	Dark blue powder
Solubility in water	Soluble in water
λ_{max} (nm)	594

sulfate pentahydrate ($CuSO_4 \cdot 5H_2O$) was purchased from Fluka AG company. Anhydrous ethanol was purchased from Carlo Erba reagents company.

The change of pH was adjusted using 1.0 M H_2SO_4 and 1.0 M NaOH solutions. The wavelength λ_{max} (nm) was specified using a spectrophotometer (UV/VIS model 1800 SHIMADZU).

2.2. Catalyst preparation

The G-Fe/Cu-NPs was prepared following the same procedures showed in the previous study [27] with some modifications as follows:

Step 1. Fresh ficus leaves were washed several times using tap water and then washed with distilled water to eliminate any impurities or dust, followed by drying in an oven at 60 °C. Additionally, they were cut using mortar and pestle into small pieces with sifting using a 2.5 mm sieve.

Step 2. The ficus leaves extract is prepared in 150 ml of deionized water with 20 g of ficus leaf pieces which were then boiled at 70 °C for 20 min and then filtered using filter paper to remove suspended ficus particles. Finally, the filtrate is refrigerated at 4 °C until used as the reducing and capping agent.

Step 3. A solution of 1.494 g of $FeSO_4.7H_2O$ and 0.7 g of $CuSO_4.5H_2O$ salts were dissolved in 100 ml of deionized water. After the salts had completely dissolved, the filtration process using a filter paper was followed to remove any impurities. To develop the synthesis of G-Fe/Cu-NPs, 100 ml of extract (Step 2) was added dropwise to the 100 ml of Fe (II) / Cu (II) mixture until the color of the mixture changed gradually from yellow, brown and finally to black indicating the metals equivalent were reduced to zero-valent and the formation of G-Fe/Cu-NPs completed. The remaining ficus extract is added to accelerate the reduction. In addition, the mixture is stirred continuously for 15 min. The black precipitate of G-Fe/Cu-NPs nanoparticles was separated by vacuum filtration using filter paper and immediately washing process was involved using distilled water several times followed by rinsing with absolute ethanol. The G-Fe/Cu-NPs were then dried overnight at ambient temperature and then ground by mortar and pestle to a fine powder.

2.3. Design of fixed-bed column

A fixed bed is a column of glass designed with a dimension of (33 cm) height and (2.2 cm) diameter which might be operated with any required height as illustrated in Fig. 1. A granular glass bead (with size 1.5–3 mm) was filled in the (9 cm) distance of the bottom and up of the column to uniform the flow of solution, whereas glass wool (1 cm thickness) was used before and after the packed bed to support this layer and prevent any material to pass down or up. The G-Fe/Cu-NPs is mixed with an amount of

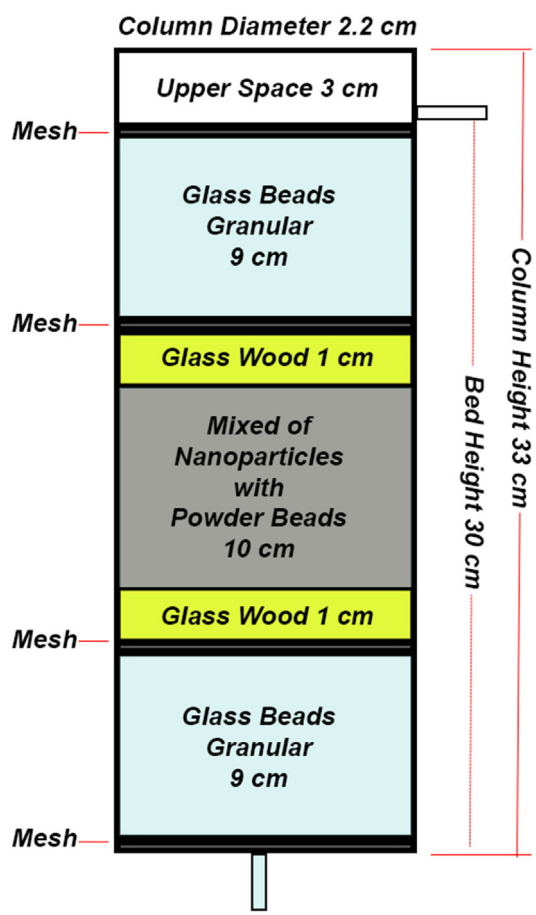

Fig. 1. The column design of continuous Fenton-like process for DB15 removal.

glass bead powder (with size <750 μm) to form a 10 cm length of the packed layer to be placed between the supported glass wool layers. The presence of powder glass beads with nanoparticles is very important to increase the retention time of the influent stream. The Intelligent Flow Pump was used to push the solution up-ward in the column. Lastly, four meshes were put in a different region for supporting function.

2.4. Characterization of G-Fe/Cu-NPs

Some techniques are utilized to prove the chemical classification, structure, size, and surface area of nanoparticles. The morphology, topography, and average size of these nanoparticles were characterized using a scanning electron microscopy (SEM) model. The EDAX technique is a confirmatory method used to ensure the identification and chemical classification of each particle. In addition, the XRD system is also utilized to investigate the crystallinity of the materials. The major picks using XRD system can accurately determine the crystalline nature of nanoparticles. Furthermore, FT-IR spectroscopy is widely used to confirm the structure of unidentified compounds, as well as to determine the functional groups of numerous materials, especially for biomaterials. The BET technique determines the specific surface area, the size radius of average pore, average porosity radius, and pore volume of nanoparticles. At last, zeta potential is widely used to inspect the potential stability of the colloid nanoparticles. The high positive or negative zeta potential for colloids tends to be stable electrically while low zeta potential for colloids is flocculated or coagulated.

2.5. Analytical methods

Before starting the experiments, a calibration curve of standard DB15 solution was done to find the maximum wavelength of dye and the relationship equation of the absorbance with concentration. Thus, the maximum wavelength of DB15 was found to be 594 nm as shown in Fig. 2, and the removal efficiency (RE) of batch experiments was calculated based on this formula:

$$RE\% = \frac{C_o - C_t}{C_o} \times 100 \quad (1)$$

where the C_o is the initial DB15 concentrations and C_t is the DB15 concentration at time t.

For the fixed-bed column, the breakthrough curve is a function of the C_t/C_o to the initial concentration versus time (t), where C_t is the effluent concentration.

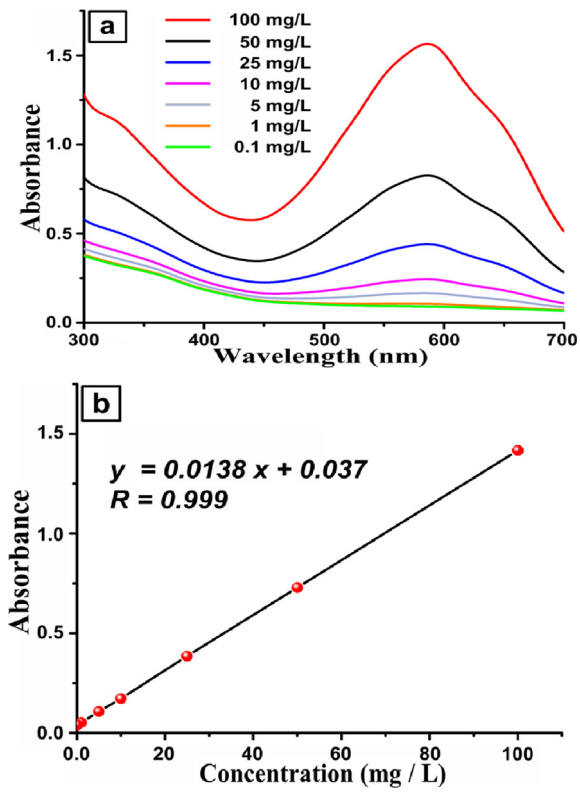

Fig. 2. UV–Vis analysis for various concentrations of DB15 solutions (a) Absorption and (b) Calibration plot.

The breakthrough time (t_b) represents the lower concentration value which is obtained from the breakthrough curve at the point that reaches the effluent concentration up to 0.001 C_t/C_o [24]. Moreover, the area under the curve can be estimated by numerical or graphical integration ways. In theory, the point that the catalyst reaches saturation or exhausted state means no dye removal happens is known as saturation time (t_s), in other way, t_s can be obtained when the effluent concentration reaches up 0.95 C_t/C_o. Further, the MTZ is the region where the contaminant is being removed, and its height (L_{MTZ}) indicates dye removal started to occur in the packed layer and can be estimated according to equation (2) [28]:

$$L_{MTZ} = L\frac{t_e - t_b}{t_e} \quad (2)$$

where L is the bed height, and t_e is the equilibrium time or the time needed for the MTZ to be established or moved completely out of the bed. Determine the total treated volume V_{eff} (ml), the following equation was used [29]:

$$V_{eff} = Q \times t_s \tag{3}$$

where Q is the solution flow rate (ml/min), and t_s is the saturation time (min).

The total removal of dye quantity q_{total} (mg) can be estimated by the equation below [29]:

$$q_{total} = \frac{QA}{1000} = \frac{QC_o}{1000} \int_{t_o}^{t_s} C_r dt \tag{4}$$

where A is the area under the curve, C_r is the removal concentration (C_o-C_t) in (mg/L), and t_s is the saturation time (min). Also, D. Charumathi and N. Das 2012 reported that the total dye fed to fixed-bed can be calculated by the equation:

$$q_{total} = \frac{C_o \times Q \times t_e}{1000} \tag{5}$$

The total quantity of dye fed to fixed-bed column m_{total} (mg) can be determined by the following equation [29]:

$$m_{total} = \frac{C_o Q t_s}{1000} \tag{6}$$

The total removal efficiency (RE %) of the fixed-bed experiments can be computed by the equation:

$$RE\% = \frac{q_{total}}{m_{total}} \times 100 \tag{7}$$

Finally, the EBCT term refers to the empty bed contact time that shows the relationship between the solute flows in the column and the catalyst [30] which can be expressed by the equations:

$$EBCT = \frac{V_C}{Q} \tag{8}$$

$$V_C = A_C Z \tag{9}$$

where V_C is the volume of catalyst in the column (m^3) and A_C is the column cross-sectional area (m^2).

2.6. Oxidative degradation of DB15 by Fenton-like in the batch experiments

In the batch mode, the ability of the Fenton-like process in DB15 degradation was evaluated under some operating conditions including H_2O_2 concentrations, G-Fe/Cu-NPs doses, pH, initial dye concentration, and temperature. The working solution of 50 mg/L of DB15 was prepared, followed by adjusting pH before adding catalyst. A known amount of G-Fe/Cu-NPs was added to the working solution and stirred for a minute to homogenize the catalyst with solution, then a certain concentration of H_2O_2 was added and stirred at 300 pm. During each run, 10 ml samples were taken regularly and mixed with prepared 200 μl of 1M Na_2SO_3 in the vial to quench the reaction. The samples were analyzed by UV/Vis after filtering the sample using a 0.22 μm membrane filter [7].

2.7. Oxidative degradation of DB15 by Fenton-like in the fixed-bed experiments

The continuous Fenton-like experiments were conducted with the optimum condition of H_2O_2 and pH that would be obtained from batch experiments. While the other operating conditions are initial DB15 concentrations in the range (25–125 mg/L), G-Fe/Cu-NPs thickness ranging from (0.5–1.5 cm), and the flow rate in the range (2–10 ml/min). Worthy to note that the thickness of powder glass beads is changed along with changing the thickness of G-Fe/Cu-NPs to maintain (10 cm) as overall thickness. Accordingly, working solution of DB15 was prepared followed by adjustment pH of the solution to the target value before adding the H_2O_2. Then the solution was pumped and regulated with a peristaltic pump to maintain the dye solution entering the column and passed through granular beads, glass wool, packed layer, glass wool, granular beads, and outlet discharge.

The flow of dye solution inside the column was continued until the collected concentration (C_t) of DB15 reached up to (⩾90%) of the initial concentration then the experiments stopped with recording the saturation time. The continuous experiments were performed at atmospheric pressure and room temperature (30–35 °C). The samples (10 ml) were collected at regulated interval time through the out effluent, filtered using 0.22 μm micro-filter, and then moved to the glass vial containing (200 μL) Na_2SO_3. Fig. 3 shows an illustration image of the Fenton-like experiments for the DB15 removal.

2.8. Design of continuous experiments

In the BBD, the optimization of variables is performed by selecting three levels of each variable (flow rate, initial dye concentration, and catalyst height) and varied over a coded value of (−1, 0, +1) in a fitting model (quadratic, linear etc.). Therefore, design-expert 13 software was employed to design, optimize, and analyze the process parameters as well as obtain an applicable model to represent dye degradation by Fenton-like using a fixed-bed column.

The second-order polynomial model based on the analysis of variance ANOVA that is suggested by

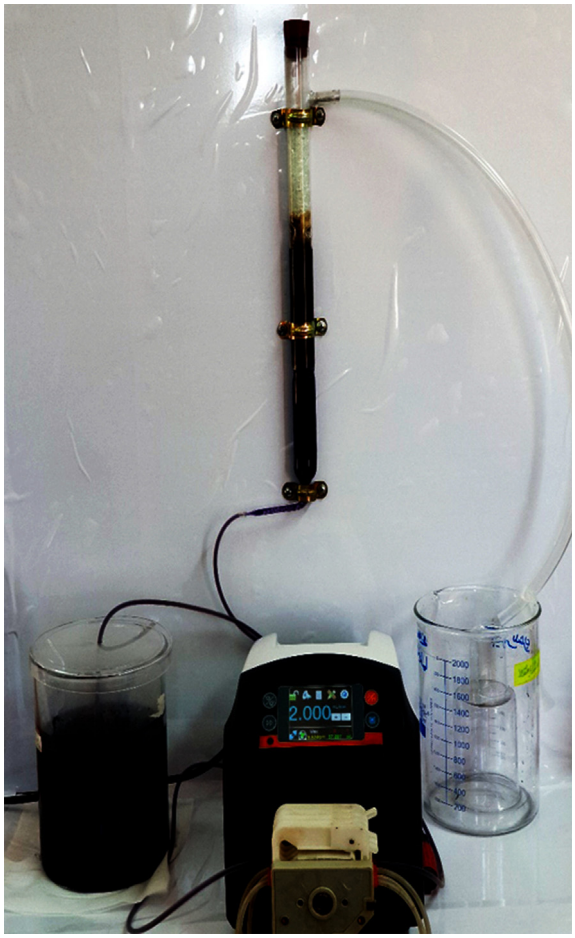

Fig. 3. The illustration image for system of continuous Fenton-like process for DB15 removal.

the design software for the three studied parameters can be illustrated in equation (10).

$$y = b_o + \sum b_i X_i + \sum b_{ii} X_i^2 + \ldots + \sum \sum b_{ij} X_i X_j \quad (10)$$

where y is a predicted response (dye removal percentage), i is 1, 2, 3, j is also 1, 2, 3, b_o is the constant coefficient, b_i and b_{ii}, are model coefficients, b_{ij} interaction coefficient, and X is coded variable. At last, the fitness of the polynomial model is examined by the coefficient R^2. In this study, the BBD is including 15 runs that are listed in Table 2.

3. Results and discussion

3.1. Formation and characterization of G-Fe/Cu-NPs

The SEM images in Fig. 4 showed that synthesized G-Fe/Cu-NPs were porous and shaped as spherical with diameters ranging from 32 to 59 nm. These nanoparticles structure can improve the dye removal rate due to improving the catalytic activities. The size variation of NPs created is due to the variation of the local concentration of the ficus extract which is responsible to reduce the metal ions.

The EDAX spectrum of nanoparticles presented in Fig. 5 contains further information about the synthesis of G-Fe/Cu-NPs. The findings of atomic distribution on the surface and chemical composition was demonstrated by the intense peaks of Fe, Cu, C, and O, 5.51 wt%, 3.33 wt%, 48.67 wt%, and 42.49 wt %, respectively. The finding of adjoint elements such as C and O signals resulted mainly from the

Table 2. Box-Behnken design experiments variables in actual and coded values.

Run No.	Actual variables			Coded variables		
	Flow rate (ml/min)	Initial concentration (mg/L)	G-Fe/Cu-NPs height (cm)	X_1	X_2	X_3
1	10	125	1	1	1	0
2	10	25	1	1	−1	0
3	10	75	1.5	1	0	1
4	10	75	0.5	1	0	−1
5	6	75	1	0	0	0
6	6	75	1	0	0	0
7	6	75	1	0	0	0
8	6	25	0.5	0	−1	−1
9	6	25	1.5	0	−1	1
10	6	125	1.5	0	1	1
11	6	125	0.5	0	1	−1
12	2	125	1	−1	1	0
13	2	25	1	−1	−1	0
14	2	75	0.5	−1	0	−1
15	2	75	1.5	−1	0	1

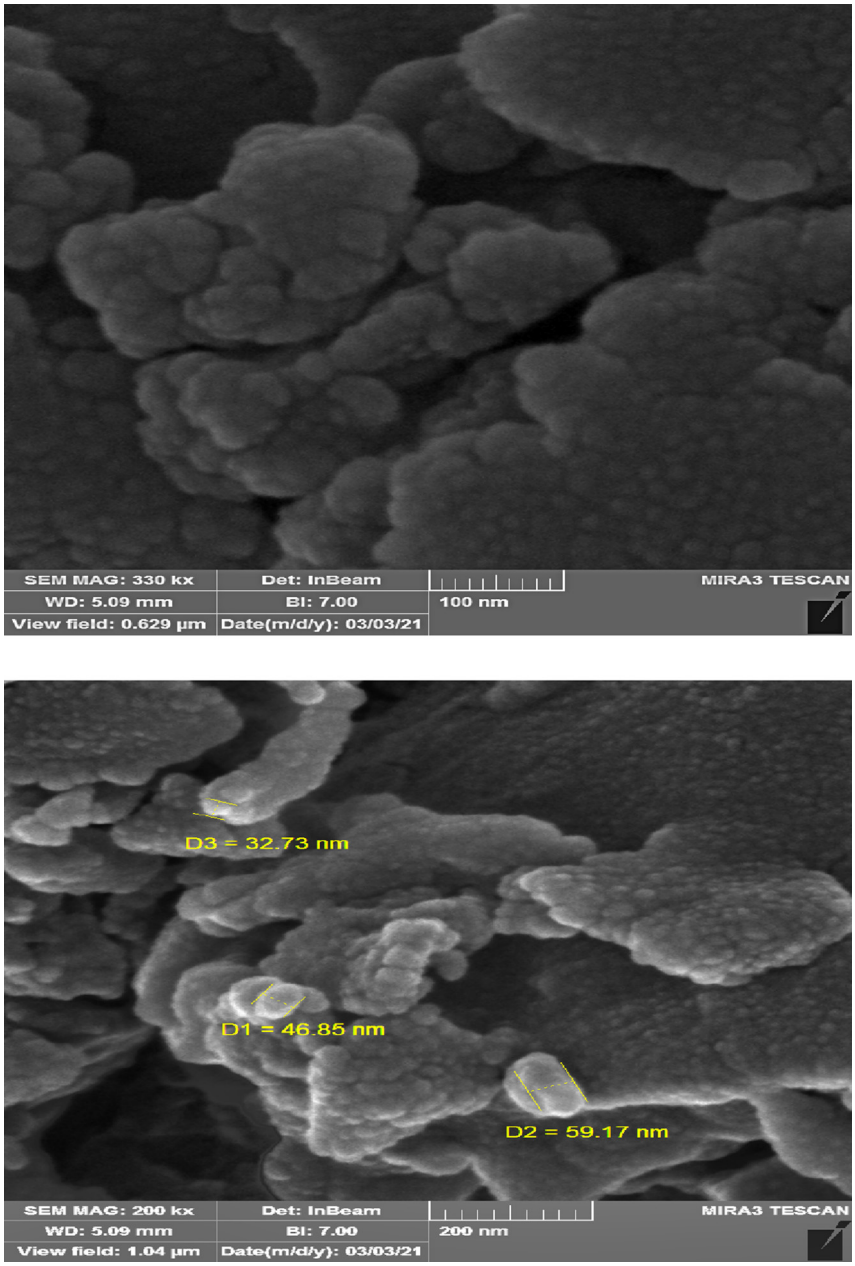

Fig. 4. SEM images of G-Fe/Cu-NPs.

ficus extracts that contain organic compounds C and O molecules which play a major role in the reduction and stabilizing process of G-Fe/Cu-NPs [22].

The XRD curve of synthesized nanoparticles is revealed in Fig. 6 which does not include any sharp peaks, indicating there is no crystal structure, even with a wide range of diffraction peaks (from 20°-25°). The above result proves that the G-Fe/Cu-NPs prepared by the green method are amorphous [31].

Before the reaction, FT-IR for ficus leaves was already applied in the band range 400–4000 cm^{-1} as shown in Fig. 7-a. Then, the functional groups of these nanoparticles were proved by conducting FT-IR analysis for band range 400–4000 cm^{-1} to ensure the functional group of these nanoparticles as depicted in Fig. 7-b. The O–H stretching vibrations illustrated in the band between 3220 and 3430 cm^{-1} belong to polyphenol compounds which play an important role to reduce the Fe/Cu metals and help to synthesize bimetallic nanoparticles [22]. The amide group in the prepared nanoparticles can be noticed at band 1614 cm^{-1} which indicates the presence of flavonoids, polyphenols and proteins in ficus leaf, these compounds attribute to reducing the

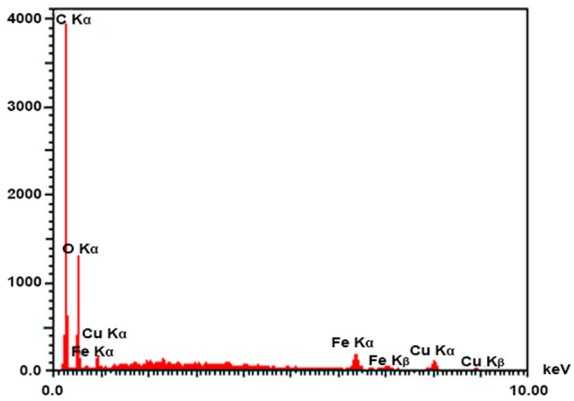

Fig. 5. EDAX of prepared G-Fe/Cu-NPs sample.

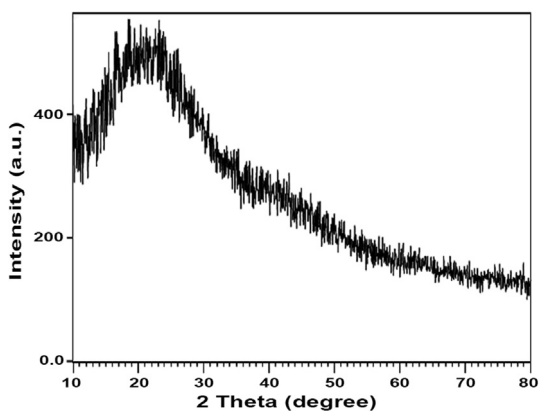

Fig. 6. XRD of prepared G-Fe/Cu-NPs sample.

formation of G-Fe/Cu-NPs [32]. The C=C sequences at 1446 cm^{-1} are attributed to the aromatic ring, while the bands at 1396 and 1244 cm^{-1} are related to C–OH bending [33]. The band observed at 823 cm^{-1} is related to the (Fe–O–Fe) stretching, and the vibration broadband ranged between 549 and 403 cm^{-1} could be assigned as Fe/Cu nanoparticles [34].

The peaks ranging from 1174 to 1070 cm^{-1} are caused by the carbonyl groups (C–O–C) stretching, these groups can prevent nanoparticles agglomeration by producing capping agents [35]. The phenolic compounds of ficus leaf extract adsorbed on the prepared nanoparticles were confirmed by the mentioned peaks. Furthermore, these phenolic compounds provide more stability to the nanoparticles when they are adsorbed on the surface and act as a capping agent [36]. As a result, The FT-IR analysis proved the ability of the ficus leaf for doing the stabilizing and reducing functions for G-Fe/Cu-NPs.

Table 3 shows the results of G-Fe/Cu-NPs surface area obtained by the BET technique. In this analysis, the pore size of G-Fe/Cu-NPs was 40.4 nm which can be classified as mesoporous according to the classification of the IUPAC. Mesoporous structure enhances the catalytic activities due to enhancing the diffusion materials. These size pores provide more stability by acting as a shielding agent to prevent the harsh reaction conditions of the nanoparticles active sites [34].

The high value of zeta potential provides the stability to nanoparticles for resisting aggregation, while the small potential leads to flocculation. As shown in Fig. 8, a high negative value at (−51.47 mV) was obtained from zeta potential analysis provides good stability of G-Fe/Cu-NPs, this stability derives from existing phenolic compounds in the ficus leaf extract [37].

3.2. Optimizing of Fenton-like factors in the batch mode

3.2.1. Effect of H_2O_2 concentration

Determining the optimal concentration of H_2O_2 is an important step in the Fenton-like. Therefore, several experiments for DB15 degradation were conducted by varying the concentration of H_2O_2 in the range (1.7–5.28 mmol/L) with fixing the other factors of G-Fe/Cu-NPs, initial DB15 concentration, pH, and temperature. The removal efficiencies of DB15 were 30.9%, 47.1%, 72.8%, 65.8%, and 56.6% for the H_2O_2 concentrations of 1.7, 2.64, 3.52, 4.4, and 5.28 mmol/L respectively for 120 min reaction time as depicted in Fig. 9. The increase of H_2O_2 concentration had a positive impact on the DB15 degradation that attributed to the production of a higher amount of very reactive ·OH radicals which is responsible to degrade dyes molecules. Nevertheless, the excess amount of hydrogen peroxide worked as inversely effect on the degradation rate, this phenomenon ascribed to ·OH scavenging and produce the lower reactive $\bullet O_2H$ radicals as illustrated in the following mechanism [38]:

$$H_2O_2 + \bullet OH \rightarrow H_2O + \bullet O_2H \quad (11)$$

All in all, the concentration of 3.52 mmol/L was selected as the best H_2O_2 concentration and would be used for the subsequent experiments. A similar result was observed by Ref. [16].

3.2.2. Effect of catalyst doses

The batch experiments of DB15 degradation by the Fenton-like were carried out using 50 mg/L of DB15 with various doses ranging (0.4–1.6 g/L) of G-Fe/Cu-NPs and maintaining the other experimental conditions fixed (Fig. 10). The removal rate of DB15

were 65.8%, 74.7%, 77.6%, 75%, and 72.4% for doses 0.4, 0.7, 1.0, 1.3, and 1.6 g/L respectively at 120 min.

The degradation rate of DB15 increased slightly with a higher amount of G-Fe/Cu-NPs due to providing a higher quantity of active sites on the surface of the catalyst which in turn contribute to producing plenty of ·OH radicals. However, this increase is limited to a specified range for the agglomeration reason occurred with high catalyst concentration which led to clogging the active sites and thereby lowering the degradation rate [39]. Despite the higher degradation rate of the 1 and 1.3 g/L, the 0.7 g/L have been chosen because of it is a cost-effective amount.

Table 3. BET parameters for G-Fe/Cu-NPs.

Parameter	Value
BET (m^2/g)	4.452
Pore size (nm)	40.4
Pore volume (cm^3/g)	0.0108

3.2.3. Effect of pH on the DB15 degradation

The pH impact on the degradation of DB15 was investigated by changing the pH of the solution in the range 2–7 while keeping the other factors constant (Fig. 11). The DB15 removal efficiencies were 77.3, 97.6, 74.7, 40.9, and 36% at various pH 2, 3, 4, 5, and 7 along with 120 min. It can be observed a

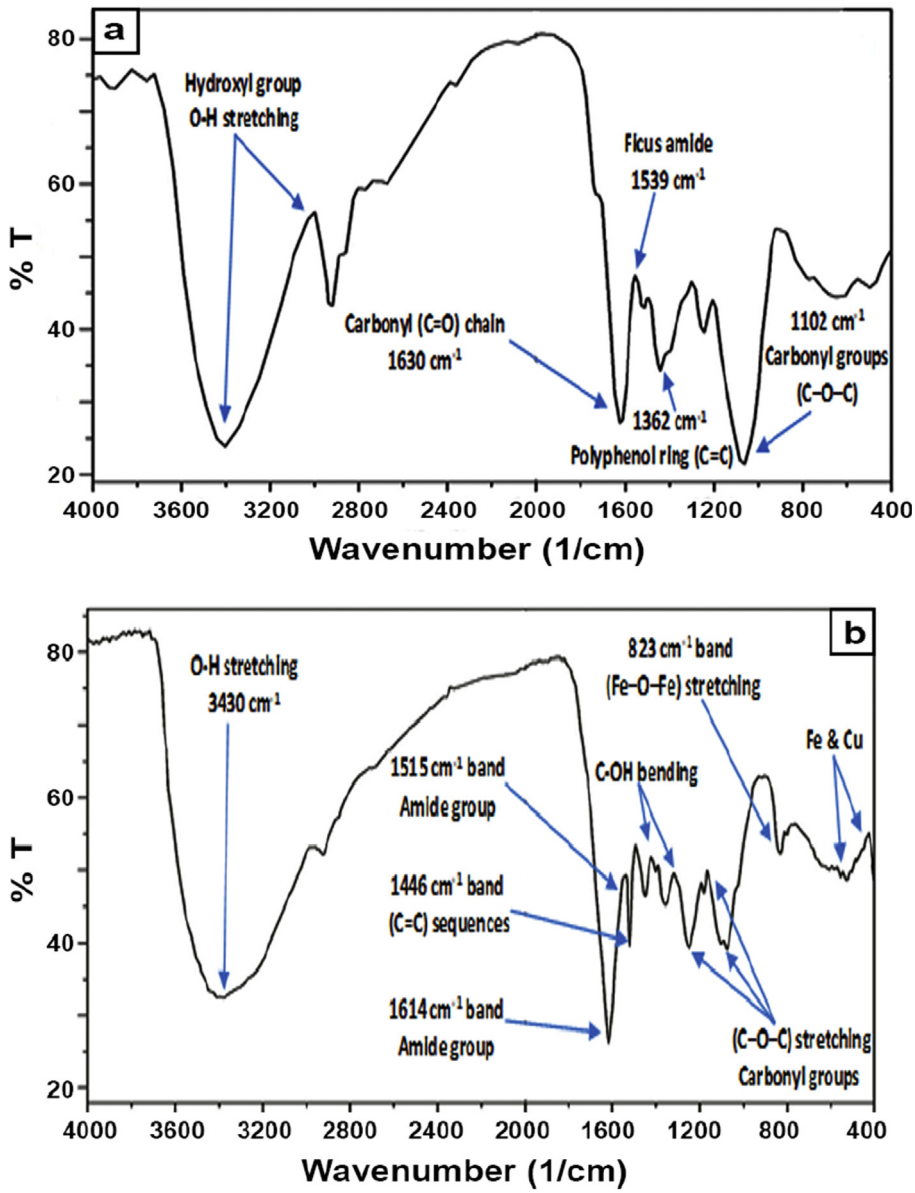

Fig. 7. FTIR spectrum of (a) dry ficus leaves (b) prepared G-Fe/Cu-NPs samples.

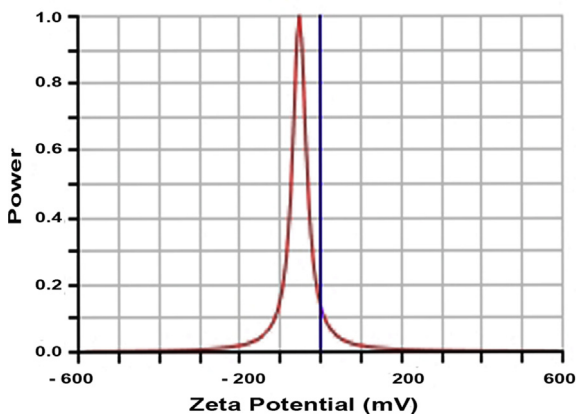

Fig. 8. Zeta potential analysis for a sample of G-Fe/Cu-NPs.

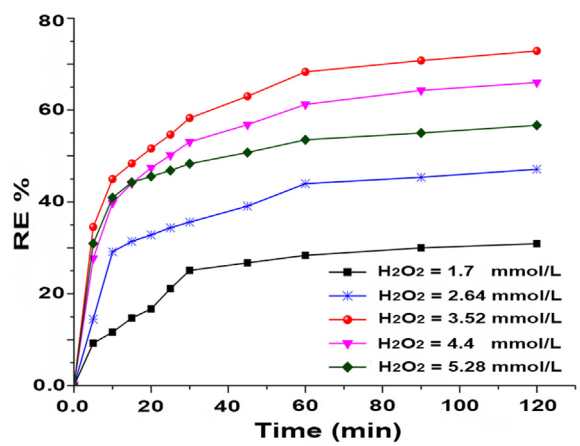

Fig. 9. Effect of H_2O_2 concentration at the dose of G-Fe/Cu-NPs, initial DB15 concentration, pH, and temperature were 0.4 g/L, 50 mg/L, 4, and 30 °C.

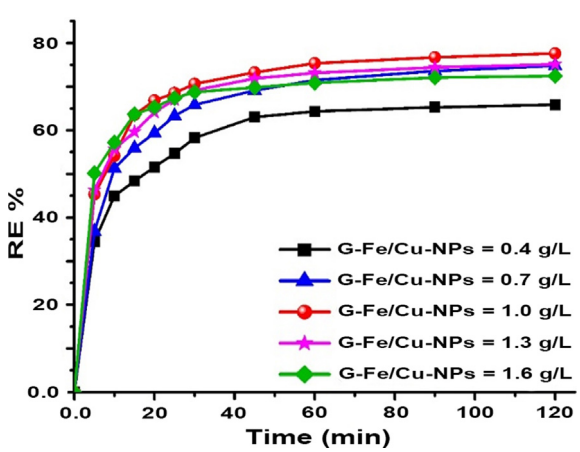

Fig. 10. Effect of G-Fe/Cu-NPs dosage at H_2O_2 concentration, initial DB15 concentration, pH, and temperature were 3.52 mmol/L, 50 mg/L, 4, and 30 °C.

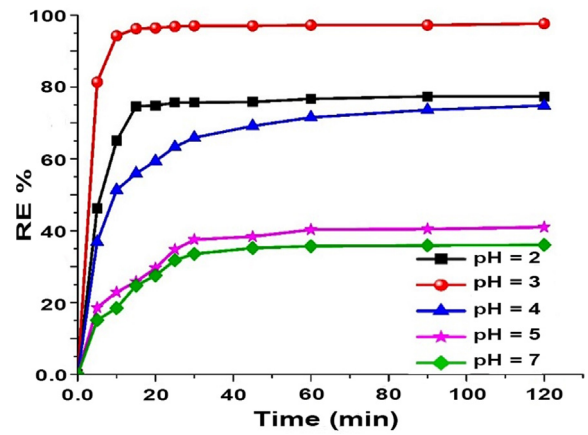

Fig. 11. Effect of pH on the DB15 degradation at G-Fe/Cu-NPs dosage, H_2O_2 dose, initial concentration, and temperature, were 0.7 g/L, 3.52 mmol/L, 50 mg/L, and 30 °C.

significant effect of pH on the DB15 degradation where the rapid degradation rate started at the beginning of experiments (within the first 15 min) indicated the fast conversion of hydrogen peroxide to ·OH. Therefore, the degradation performance decreased as the pH increased due to low amount of reactive components such as $Fe(OH)_3$ that has the capability to deactivate the catalyst and thereby lowering the number of ·OH radicals [40]. In contrast, the degradation performance decreased at pH 2 because of the extra protons (H^+) that scavenged •OH radicals according to the below reaction [41].

$$\bullet OH + H^+ + e^- \rightarrow H_2O \tag{12}$$

Therefore, the most effective pH was approximately 3. The pH result was consistent with earlier reported by Ref. [41].

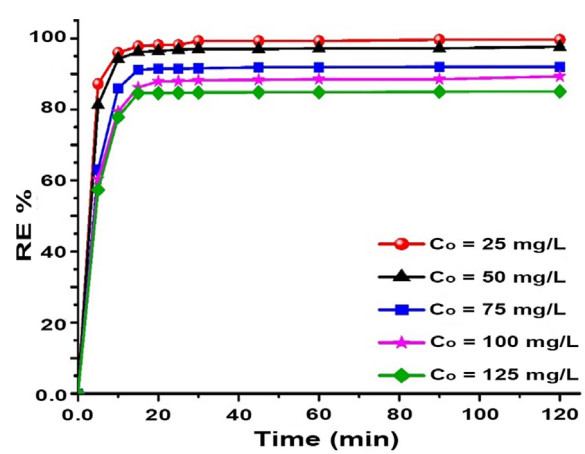

Fig. 12. Effect of initial DB15 concentration at G-Fe/Cu-NPs dosage, H_2O_2 concentration, pH, and temperature were 0.7 g/L, 3.52 mmol/L, 3, and 30 °C.

3.2.4. Effect of initial dye concentration on the degradation performance

In the Fenton-like process, several concentrations of DB15 (25, 50, 75, 100, and 125 mg/L) were studied to illustrate the impact of initial DB15 concentration on the degradation rate. The result shows that when the initial concentration of DB15 was raised, the removal efficiency dropped from 95.9%, 94.2%, 85.9%, 79.3% and 77.8% respectively within 15 minutes of reaction time (Fig. 12). The degradation performance is limited by the number of very reactive ·OH radicals that exist in the medium, where the higher concentration required more hydroxyl radicals. Further, the Fenton-like reaction could generate by-products that tried to compete with the dye molecules for occupying the catalytic active sites resulting in decreased degradation rate [39]. As a result, the concentration of 100 mg/L was chosen as the more suitable DB15 concentration and used with the following experiments. Similar results are reported by Ref. [42].

3.2.5. Effect of temperature on the degradation performance

The degradation of DB15 was evaluated by varying reaction temperature between (20–50 °C) while other factors were fixed. The degradation rates were 85.5%, 89.3%, 97.7%, and 98.7% for the temperature 20, 30, 40, and 50 °C respectively within 120 min (Fig. 13).

Rising temperature from 20 to 30 °C within the first 15 min of reaction leads to an increase in the degradation efficiency of DB15 from 82.8 to 96.6%. The positive effect of the high temperature is ascribed to the relatively high production of hydroxyl radicals as well as the enhancement of collisions between the ·OH and DB15 molecules that accelerated the rate of reaction [14]. Meanwhile, the excessively higher temperature may lead to the decomposition of hydrogen peroxide and then lowering the efficiency of degradation [7]. However, the temperature of 50 °C was chosen as the best operational temperature. This behavior was in good agreement with a previous study reported by Ref. [43].

3.3. Experimental design of DB15 degradation in the fixed-bed column

The inert materials have been tested individually and as a group (without catalyst" to check if there is any effect or removal of the dye. The dye solution with known initial concentration was pumped up into the column, then the outlet samples were collected and compared with feed concentration. The results deduced that the inert materials had neither effect nor removal of dye. Also, the effect of H_2O_2 only was checked with the same previous step by comparing the initial concentration with the out concentration, and the result showed no effect on dye removal. After that, the real fixed-bed experiments were accomplished by varying the flow rate from (2–10 ml/min), initial concentration of (25–125 mg/L), and catalyst thickness of (0.5–1.5 cm). Notably, the thickness of powder glass beads is changed along with the changing the thickness of G-Fe/Cu-NPs to maintain (10 cm) as overall thickness. Meanwhile, the other operation factors were maintained at H_2O_2 of 3.52 mmol/L, and pH of 3 along with the experiments. The removal efficiency was calculated using equation (7).

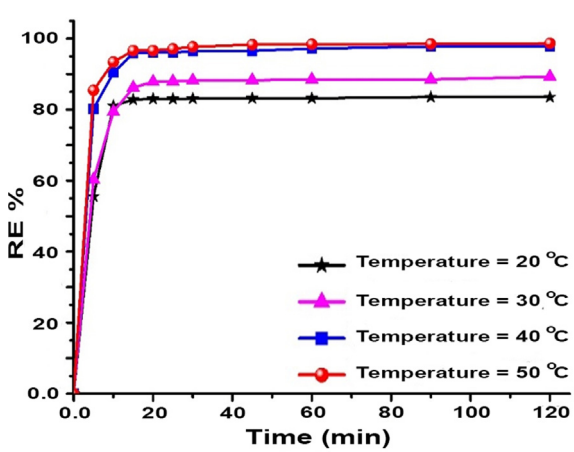

Fig. 13. Effect of temperature on the removal DB15 at G-Fe/Cu-NPs dosage, H_2O_2 concentration, initial dye concentration, and pH were 0.7 g/L, 3.52 mmol/L, 100 mg/L, and 3.

Table 4. Experimental and predicted response in the Box-Behnken for the DB15 degradation.

Run No.	Experimental result %	Predicted response %	Deviation
1	22	21.88	0.12
2	39	39.38	0.38
3	31	32.63	1.63
4	32	32.33	0.33
5	56	57.13	1.13
6	22	23.25	1.25
7	32	32.33	0.33
8	32	33.5	1.5
9	33	32.33	0.67
10	42	40.5	1.5
11	44	44.13	0.13
12	45	43.75	1.25
13	31	30.63	0.37
14	29	27.88	1.12
15	36	34.38	1.62

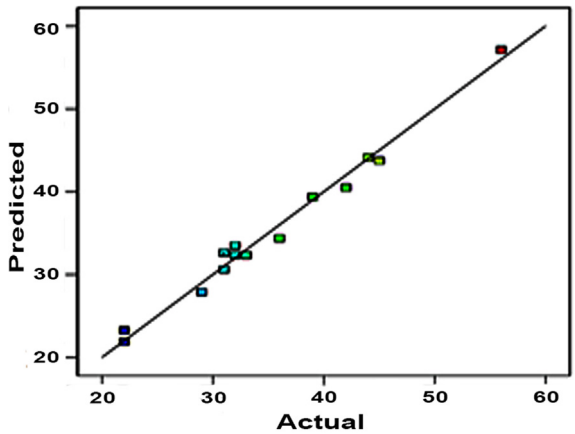

Fig. 14. Actual versus Predicted values for the degradation DB15 designed experiments.

3.3.1. DB15 degradation experimental design

By the created BBD, the experimental data were compared with the adjusted and predicted values that were analyzed statistically by the software (Table 4), hence, the obtained correlation coefficient R^2 was 0.985 that showing fit excellently of experimental data with the suggested model. Furthermore, Fig. 14 showed the significance of the suggested model by plotting the experimental vs predicted values that showed identical fit. Besides, the model equation for the removal of dye in the fixed-bed column can be mathematically stated according to equation (13):

$$y = 76.479 - 6.875X_1 - 0.463X_2 + 2.833X_3 + 0.022X_1X_2 + 0.875X_1X_3 + 0.04X_2X_3 + 0.216X_1^2 + 0.0009X_2^2 - 2.167X_3^2 \quad (13)$$

where y is the response (removal rate %), X_1 is the flow rate (ml/min), X_2 is the initial dye concentration, and X_3 is the height of G-Fe/Cu-NPs.

3.3.2. Analysis of variance results

The analysis of variance (ANOVA) is a perfect analysis for evaluating the quality of the fitted

Table 6. The optimizing model of DB15 degradation.

Parameter	Optimum value
X_1 – Flow rate (ml/min)	2.13
X_2 – Initial DB15 concentration (mg/L)	26.16
X_3 – Catalyst height (cm)	1.42
Actual response % (removal efficiency %)	56
Predicted response % (removal efficiency %)	56.35
Error %	0.35

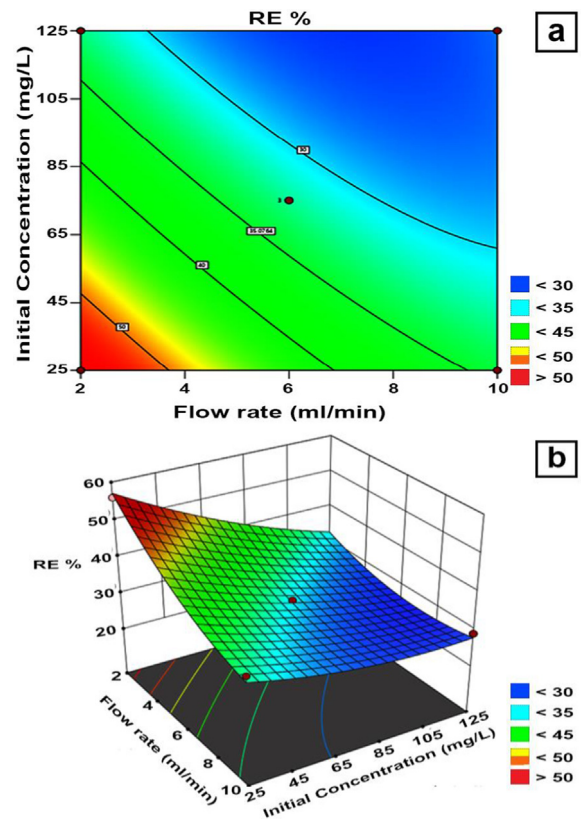

Fig. 15. Effect of interaction between flow rate and initial DB15 concentration on removal response at pH = 3, H_2O_2 = 3.52 mmol/L, temperature = 30 °C, and pressure = atmosphere pressure (a) contour plot (b) 3D surface response.

Table 5. Experimental and predicted response in the Box-Behnken for the DB15 degradation.

Factor	Sum of Squares	df	F-value	P-value	Comments
X_1-Flow rate	378.13	1	115.16	0.0001	Significant
X_2-Initial dye concentration	480.50	1	146.35	<0.0001	Significant
X_3-Catalyst height	91.13	1	27.75	0.0033	Significant
X_1 X_2	81.00	1	24.67	0.0042	Significant
X_1 X_3	12.25	1	3.73	0.1113	
X_2 X_3	4.00	1	1.22	0.3200	
X_1^2	44.16	1	13.45	0.0145	
X_2^2	18.01	1	5.48	0.0662	
X_1^2	1.08	1	0.3299	0.5906	
Lack of Fit	15.75	3	15.75	0.0603	Not significant
Pure Error	0.6667	2			
Total	1124.9	14			

model. However, the polynomial model based on the ANOVA is suggested by the design software. The ANOVA quadratic model data is shown in Table 5. This table shows the significant influences of the studied variable on the removal by determining the probability of results (P-value) and F-value, notably, the model is being significant when the P-value is < 0.05 and F-value is large [44].

3.3.3. Process optimization

The accuracy of the model was verified by the optimized studied factors of DB15 removal. The result showed that the error between experimental results and the predicted value was 0.35 as shown in Table 6, thus, the model efficacy was confirmed.

3.3.3.1. Interaction effect of flow rate and initial dye concentration. The plot in Fig. 15a for flow rate versus initial concentration represents the contour design of 2-dimensional concerning removal response. On the other hand, the 3-dimensional graph illustrated in Fig. 15b refers to the interaction impact of initial concentration with catalyst height on the DB15 degradation rate response. A significant effect in the interaction between flow rate and initial DB15 concentration can be seen from the two plots. When the flow rate was lower than 2.5 ml/min, the initial DB15 concentration had a strong effect on the response, on the other hand, the flow rate was the most significant with the high levels of the initial concentration. However, the uptake and removal efficiency for dye decreased with increasing flow rate and the higher value is shown at a low flow rate.

This phenomenon was possibly related to reducing the resident time between DB15 solution and catalyst at a higher flow rate, while it has more time to oxidize onto catalyst and complete the removal process with delay the exhaustion of the column. However, the reason for the poorly removal rate at high DB15 concentration may be attributed to the shortage production of free radicals (·OH) that work as destroying the dye molecules, indicating the importance of this parameter to initiate free radical ·OH [45]. Finally, since both parameters have played an important role in the fixed-bed column, it should be noted that the effect of initial concentration has the most significant effect with the minimum P-value and larger F-value analyzed in Table 5. As a result, the maximum removal of dye was seen at the flow rate of 2 ml/min and an initial DB15 concentration of 25 mg/L.

3.3.3.2. Interaction effect of flow rate and G-Fe/Cu-NPs height. Fig. (16a,b) show a 2-dimensional contour

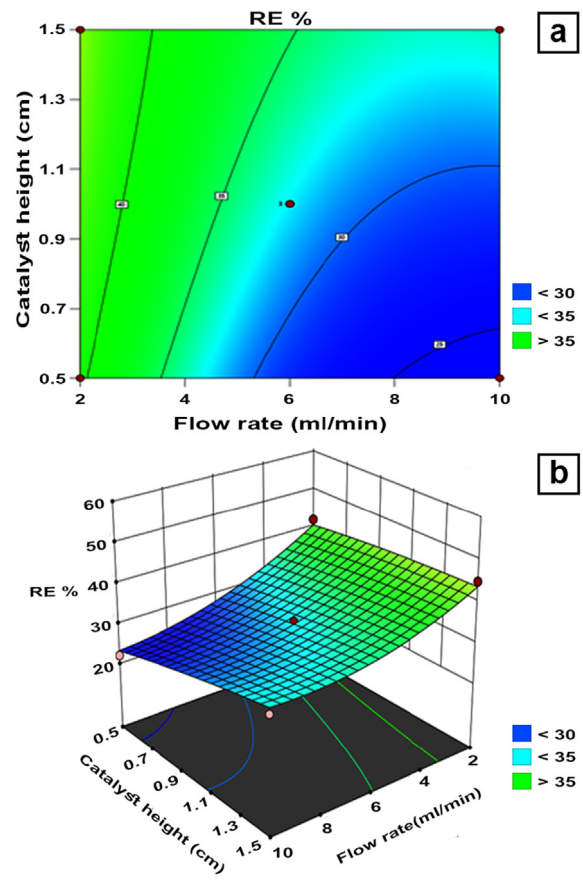

Fig. 16. Effect of interaction between flow rate and catalyst height on the removal response at H_2O_2 = 3.52 mmol/L, pH = 3, temperature = 30 °C, and pressure = atmosphere pressure (a) contour plot (b) 3D surface response.

plot of reaction response and the 3-dimensional surface plot for flow rate and catalyst height interaction and their effect on the degradation rate response of DB15.

The interaction between flow rate and catalyst height can be observed at the flow rate below 6 ml/min. Further, the plots demonstrate that the increase in catalyst bed height led to slightly increasing the removal rate, due to increasing the surface area, thereby, the availability of longer contact time between nanoparticles and DB15, also, the suitable height of catalyst resulting in a positive motivation for the formation of ·OH radicals through the transferring of electrons from G-Fe/Cu-NPs to hydrogen peroxide [45]. Furthermore, it is interesting to observe that at the catalyst height in the range of (1.3–1.5 cm) the removal efficiency was generally similar indicating the uselessness of adding more catalyst than these values, the reason could be ascribed to continuous leaching of G-Fe/Cu-NPs. In addition, the P-value and F-value in Table 5 proved that the

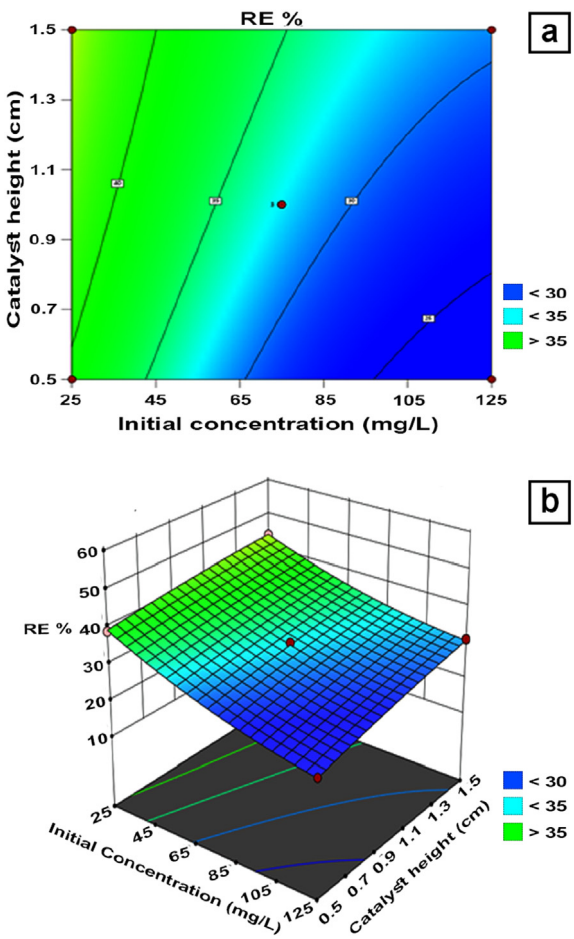

Fig. 17. Effect of interaction between initial dye concentration and catalyst height on the removal response at pH = 3, H_2O_2 = 3.52 mmol/L, temperature = 30 °C, and pressure = atmosphere pressure (a) contour plot (b) 3D surface response.

flow rate has greater significance than catalyst height.

3.3.3.3. Interaction effect of initial concentration and G-Fe/Cu-NPs height. The plot in Fig. 17a for initial concentration versus catalyst height represents the contour design of 2-dimensional concerning removal response. On the other hand, the 3-dimensional graph illustrated in Fig. 17b refers to the interaction impact of initial concentration with catalyst height on the DB15 degradation rate response.

3.3.4. Fixed-bed parameters estimation

Various breakthrough factors were determined in the fixed-bed column to verify the performance of the used column. Table A (in the appendix) summarizes the breakthrough experimental parameters obtained from the runs of the continuous degradation of DB15 by the Fenton-like process catalyzed by G-Fe/Cu-NPs. All the parameters tabulated in Table A indicated that as the flow rate and initial DB15 concentration increased, the removal rate decreased. Also, increasing of the catalyst height and decreasing flow rate led to an increase in the empty bedtime EBCT. Notably, the saturation time (t_s) increased at the lower flow rates due to saturation of the active sites on the G-Fe/Cu-NPs rapidly. Besides, the exhaust time (t_e) enhanced with decreasing the flow rate due to increasing the contact time between DB15 particles with the G-Fe/Cu-NPs active sites. On the other hand, the breakthrough time (t_b) was also influenced by the increasing flow rates when it decreased significantly due to reducing the time for diffusing dye molecules into G-Fe/Cu-NPs sites [46]. Therefore, the high level of flow rate led to lowering the total removal performance. The same result was found by Ref. [30].

As a result, Table 7 introduces the comparing results of previous studies and the present study for the removal of dyes by continuous experiments.

3.3.5. Kinetic of degradation DB15 by Fenton-like reactions in the batch mode

The kinetic of Fenton-like reaction can be described as a very complicated process that contains numerous steps that are usually fulfilled simultaneously [47]. In the Fenton-like process, the three kinetics models including zero-order, first-order, and second-order [48] were studied to estimate the DB15 degradation data.

Therefore, the removal kinetics of DB15 by the Fenton-like process was studied at the various experimental conditions such as concentration in the range of (25–125 mg/L), H_2O_2 concentration (1.7–5.28 mmol/L), the dosage of G-Fe/Cu-NPs (0.4–1.6 g/L), pH (2–7), and temperature (20–50 °C) respectively. The most studied experiments of DB15 degradation demonstrated that a greater number of hydroxyl radicals were generated at the first stage of the reaction precisely in the time range (0–15 min), after that, the reaction progress continued slowly. Thus, the first step of the process was considered in the kinetic investigation. In order to investigate the above kinetics, Table 8 shows the kinetic equations were used:

The value of k_o can be calculated from the slope of the C_t against t, and the determination of the regression coefficient is listed in appendix A (Table B). It can be seen that the values regression coefficient R^2 for all studied parameters of this model was not high enough, indicating that the degradation of DB15 was poorly fitted with the zero-order model. On the other hand, k_1 value can be obtained from

Table 7. Results of a previous and present studies for the removal of dyes by continuous experiments.

No.	Dye	Optimum factors and major results	References
1	methyl orange	Dye conversion = 99.4% Flow rate = 4 ml/min Catalyst amount = 3.5 g C_o = 50 mg/L H_2O_2 = 17.6 mM Fixed-bed height = 80 mm Fixed-bed diameter = 20 mm	[49]
2	Benzylformic acid	Flow rate range = 2.5–3.5 ml/min Bed height = 10–20 cm C_o. = 9.53–13.47 mg/L Fixed-bed height = 30 cm Fixed-bed diameter = 1.2 cm	[30]
3	Methylene blue	Efficiency = 70% Flow rate range = 10 ml/min Catalyst height = 2 cm C_o = 100 mg/L H_2O_2 = 0.1633 M Fixed-bed height = 15 cm Fixed-bed diameter = 2.5 cm	[50]
4	Raw effluent from a textile mill	Efficiency = 70% (Continuous), 100% (Batch) Flow rate = 300 L/h Fixed-bed height = 20 cm Fixed-bed diameter = 4 cm Dose = 0.52 cm	[51]
5	methyl green dye	Efficiency = 52.94% Flow rate = 0.8 ml/min Fixed-bed height = 35 cm Fixed-bed diameter = 0.7 cm Bed height = 6 cm C_o = 20 mg/L	[28]
6	Direct blue 15	Efficiency = 56.35% Continuous (98.7% Batch) Flow rate = 2.13 ml/min Catalyst height = 1.26 cm, (0.7 g) C_o = 26.16 mg/L, (100 mg/L) H_2O_2 = 3.52 mM Fixed-bed height = 33 cm Fixed-bed diameter = 2.2 cm	Present study

the intercept and slope of the natural logarithm of C_t versus t. Table B shows the parameters of the first-order along with the corresponding correlation coefficient for all factors. It can be observed that the first-order has a good regression factor R^2 for all studied factors. For the second-order kinetic model, the value of k_2 can be calculated from the slope and intercept of the $1/C_t$ versus t graph. It can be seen from Table B that the linear fitting value of the regression coefficient R^2 for second order is higher than those for zero-order and first-order, which indicates that the second-order kinetic model is the fitted model for DB15 kinetic degradation by Fenton-like process catalyzed by G-Fe/Cu-NPs. Further, Fig. 18 shows the second-order kinetics for all studied parameters.

As shown in Table B that increasing of initial DB15 concentration from (25–125 mg/L) led to a decrease in the rate (0.152–0.004 $M^{-1}.min^{-1}$) which was attributed to lowering the hydroxyl radicals within increasing the DB15 concentration. Besides, as the concentration of H_2O_2 increased from (1.7–3.52

Table 8. Kinetic equations.

Model	Equation	Parameters
Zero-order	$C_t = C_o - k_o\, t$	k_o: zero-order rate constant (M. min^{-1}). *t: time (min)*
First-order	$ln\ C_t = ln\ C_o - k_1\, t$	k_1: first-order rate constant (min^{-1})
Second-order	$[1/C_t] - [1/C_o] = k_2\, t$	k_2: second-order rate constant (M^{-1}. min^{-1})

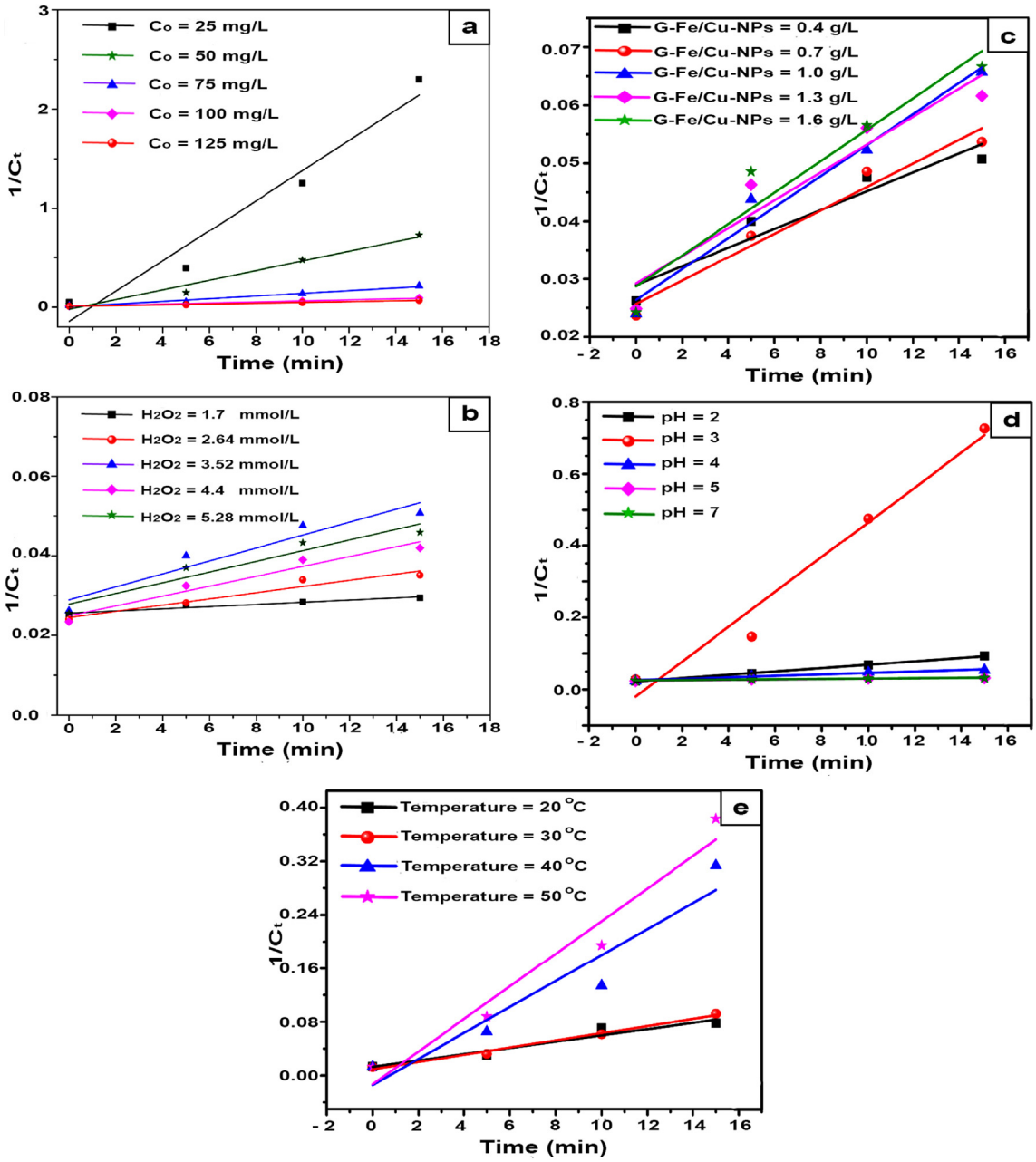

Fig. 18. Second-order kinetic analysis for (a) initial DB15 concentration, (b) H_2O_2 concentration, (c) G-Fe/Cu-NPs doses, (d) pH, (e) temperature, and (f) co-existing inorganic salts.

mmol/L) the removal of DB15 increased and that ascribed to increase the ·OH. In contrast, the excess amount of peroxide (from 3.52 to 5.28 mmol/L) led to decrease in the rate constant for the reason of ·OH scavenging. Additionally, the high amount of catalyst results in an increase in the degradation rate due to an increase in the concentration of ·OH. Otherwise, high G-Fe/Cu-NPs concentrations had resulted in a decrease of degradation rate, this was attributed to scavenging the ·OH by the high amount of Fe^{+2} [38]. Further, the second-order kinetic rate decreased from (0.152–0.004 M^{-1}. min^{-1}) as the pH increased from (2-7) due to the charges attraction between G-Fe/Cu-NPs and the DB15 molecules at low pH resulting in an easy-conducted removal reaction [7]. Furthermore, the k_2 increased by increasing the temperature where the reaction between G-Fe/Cu-NPs and H_2O_2 increased with higher temperature thereby the formation of ·OH increased [7].

4. Conclusions

This study introduces a promising approach to synthesis bimetallic iron/copper nanoparticles with high performance to remove dyes from wastewater by Fenton-like processes. Iron/copper nanoparticles were prepared by green synthesis using the extracts of ficus leaves and employed to remove the direct blue 15 dye. The G-Fe/Cu-NPs were characterized using SEM, zeta potential, XRD, AFM, BET, EDAX, and FT-IR. Therefore, the good stable, amorphous, rounded and shaped like spherical of G-Fe/Cu-NPs were found with the size range 32–59 nm, and the surface area was 4.452 m^2/g. Then, the G-Fe/Cu-NPs was performed with a complete batch and continuous processes including optimizing all required parameters. As a result, the G-Fe/Cu-NPs shows a positive effect in term of the use as a heterogeneous catalyst to remove DB15 dye where the final removal efficiency of DB15 at the optimum factors was 98.7% obtained by batch experiments and 56.35% with the continuous mode. In the batch study, the best value of the reaction parameters were (initial DB15 concentration = 100 mg/L, H_2O_2 concentration = 3.52 mM, pH = 3, catalyst dose = 0.7 g/L, and temperature = 50 °C) along with 120 min contact time. Meanwhile, the continuous parameters were studied using the Box-Behnken design and found that the optimum values of flow rate, initial dye concentration, and G-Fe/Cu-NPs depth were 2.134 ml/min, 26.16 mg/L, and 1.42 cm respectively. Moreover, the model equation for the removal of dye in the fixed-bed column was expressed by the equation:

$$y = 76.479 - 6.875X_1 - 0.463X_2 + 2.833X_3 + 0.022X_1X_2 + 0.875X_1X_3 + 0.04X_2X_3 + 0.216{X_1}^2 + 0.0009{X_2}^2 - 2.167{X_3}^2$$

Finally, the kinetic study exhibited that the second-order model was well fitted for the experimental data in the batch experiments.

Acknowledgements

The authors are highly indebted to the Department of Biochemical Engineering/al-Khwarizmi College of Engineering at the University of Baghdad, Iraq, and the Environment and Water Directorate of the Ministry of Science and Technology, Iraq, for providing all the facilities to carry out this work.

Funding

This research did not receive any specific grant from funding agencies in the public, commercial, or not-for-profit sectors.

Appendix.

Table A. The breakthrough experimental parameters

Run no.	1	2	3	4	5	6	7	8	9	10	11	12	13	14	15
Parameter															
Flow rate (ml/min)	10	10	10	10	6	6	6	6	6	6	6	2	2	2	2
Initial concentration (mg/L)	125	25	75	75	75	75	75	25	25	125	125	125	25	75	75
Catalyst height (cm)	1	1	1.5	0.5	1	1	1	0.5	1.5	1.5	0.5	1	1	0.5	1.5
Breakthrough time t_b (min)	5.02	5.1	5	5.1	8.5	8.9	11.5	8.8	8.7	9.3	9	25.5	25	26	30
Exhaust time t_e (min)	34	35	34	48	76	84	86	80	62	70	92	150	135	140	125
Saturation time t_s (min)	9.8	12.5	11	1.5	24	27	28	31	27	22	20	47	76	59	56
Volume of effluent V_{eff} (ml)	340	350	340	480	456	504	516	480	372	420	552	300	270	280	250
Maximum column capacity q_{total} (mg)	9.86	2.68	8.25	7.88	7.48	12.15	12.6	4.04	3.11	16.5	11.85	9.53	3.08	6.69	6.94
Total quantity of dye fed into column m_{total} (mg)	34.2	7.49	25.5	36	23.7	37.8	30.6	10.4	7.15	52.5	54.49	30.4	5.47	15.9	15.5
Removal efficiency RE%	28.8	35.7	32.4	22	31.6	32.14	41.2	38.8	43.6	31.4	21.74	31.3	56.3	42.1	44.8
Volume of catalyst (cm^3)	3.8	3.8	5.7	1.9	3.8	3.8	3.8	1.9	5.7	5.7	1.9	3.8	3.8	1.9	5.7
Height of mass transfer zone L_{MTZ} (cm)	0.852	0.854	1.279	0.45	0.89	0.89	0.87	0.45	1.29	1.3	0.451	0.83	0.82	0.41	1.14
Empty bed contact time EBCT (min)	0.38	0.38	0.57	0.19	0.63	0.63	0.63	0.32	0.95	0.95	0.317	1.9	1.9	0.95	2.85
Capacity of bed at break time q_b (mg/g)	2.863	0.619	1.219	2.96	0.99	1.9	2.32	1.06	0.41	2.31	4.949	2.93	0.58	2.74	1.52
Volume treated at break time V_b (ml)	50.2	51	50	51	51	53.4	69	52.8	52.2	55.8	54	51	50	52	60
Bed volume	13.21	13.42	8.773	26.9	13.4	14.05	18.7	27.8	9.16	9.79	28.43	13.4	13.2	27.4	10.5
The superficial velocity U_f (cm/min)	2.63	2.63	2.63	2.63	1.58	1.579	1.58	1.58	1.58	1.58	1.579	0.53	0.53	0.53	0.53
Residence time t_r (min)	0.38	0.38	0.57	0.19	0.63	0.63	0.63	0.32	0.95	0.95	0.317	1.9	1.9	0.95	2.85

Table B. The Zero-, First-, and Second-order kinetics parameters for the Fenton-like reaction of degradation DB15

Parameter		RE% after 15 min	RE% after 120min	Zero-order		First-order		Second-order	
				k_o (M.min^{-1})	R^2	k_1 (min^{-1})	R^2	k_2 (M^{-1}.min^{-1})	R^2
Initial	25	97.8	99.6	1.196	0.687	0.252	0.937	0.152	0.957
DB15	50	96.2	97.6	2.199	0.723	0.22	0.938	0.048	0.972
Concentration (mg/L)	75	91.1	92	3.114	0.836	0.165	0.977	0.013	0.969
	100	86.2	89.3	4.374	0.835	0.132	0.969	0.005	0.99
	125	84.5	85	5.312	0.85	0.125	0.97	0.004	0.994
Average R^2					**0.786**		**0.958**		**0.976**
H_2O_2	1.7	14.7	30.9	0.371	0.897	0.01	0.909	0.0003	0.921
Concentration (mmol/L)	2.64	31.4	47.1	0.904	0.929	0.026	0.94	0.0008	0.947
	3.52	48.3	72.8	1.188	0.825	0.04	0.875	0.0016	0.92
	4.4	44	65.9	1.229	0.881	0.038	0.921	0.0012	0.954
	5.28	44.2	56.6	1.117	0.836	0.038	0.879	0.0014	0.912
Average R^2					**0.874**		**0.905**		**0.931**
G-Fe/Cu-NPs	0.4	48.3	65.8	1.188	0.825	0.043	0.875	0.0016	0.92
Doses (g/L)	0.7	55.9	74.7	1.54	0.861	0.054	0.919	0.002	0.963
	1.0	63.5	77.6	1.665	0.836	0.064	0.917	0.0027	0.974
	1.3	59.6	75.1	1.514	0.781	0.058	0.949	0.0024	0.916
	1.6	63.6	72.4	1.636	0.775	0.064	0.855	0.0027	0.911
Average R^2					**0.816**		**0.903**		**0.937**
Initial pH	2	74.6	77.3	1.196	0.687	0.252	0.937	0.152	0.957
	3	96.2	97.6	2.199	0.723	0.22	0.938	0.048	0.972
	4	55.9	74.7	3.114	0.836	0.165	0.977	0.013	0.969
	5	25.8	40.9	4.374	0.835	0.132	0.969	0.005	0.99
	7	24.6	36	5.132	0.85	0.125	0.97	0.004	0.994
Average R^2					**0.786**		**0.958**		**0.976**
Temperature (°C)	20	82.8	83.5	4.094	0.838	0.123	0.922	0.0047	0.936
	30	86.2	89.3	4.374	0.835	0.132	0.969	0.0054	0.99
	40	95.8	97.7	4.627	0.734	0.206	0.963	0.0194	0.913
	50	96.6	98.7	4.659	0.694	0.22	0.932	0.0244	0.956
Average R^2					**0.775**		**0.946**		**0.949**

References

[1] C. di Luca, P. Massa, J.M. Grau, S.G. Marchetti, Rosa Fenoglio, Patricia Haure, Highly dispersed Fe3+-Al2O3 for the Fenton-like oxidation of phenol in a continuous up-flow fixed bed reactor. Enhancing catalyst stability through operating conditions, Appl Catal B Environ 561 (2018) 388–394, https://doi.org/10.1016/j.apcatb.2018.05.032.

[2] I. Chaari, E. Fakhfakh, M. Medhioub, F. Jamoussi, Comparative study on adsorption of cationic and anionic dyes by smectite rich natural clays, J Mol Struct 1179 (2019) 672–677, https://doi.org/10.1016/j.molstruc.2018.11.039.

[3] S. Homaeigohar, The nanosized dye adsorbents for water treatment, Nanomaterials 10 (2020) 1–43, https://doi.org/10.3390/nano10020295.

[4] A.N. Alene, G.Y. Abate, A.T. Habte, Bio-adsorption of Basic blue dye from aqueous solution onto raw and modified waste ash as economical alternative bio-adsorbent, Hindawi 2020 (2020) 1–11, https://doi.org/10.21203/rs.2.22535/v1.

[5] M.A. Atiya, M.J. M-Ridha, M.A. Saheb, Removal of aniline blue from textile wastewater using electrocoagulation with the application of the response surface approach, Iraqi J Sci 61 (2020) 2797–2811, https://doi.org/10.24996/ijs.2020.61.11.4.

[6] K.G. Ahila, B. Ravindran, V. Muthunarayanan, D.D. Nguyen, X.C. Nguyen, S.W. Chang, et al., Phytoremediation potential of freshwater macrophytes for treating dye-containing wastewater, Sustain Times 13 (2021) 1–13, https://doi.org/10.3390/su13010329.

[7] A.K. Hassan, G.Y. Al-Kindi, D. Ghanim, Green synthesis of bentonite-supported iron nanoparticles as a heterogeneous Fenton-like catalyst: kinetics of decolorization of reactive blue 238 dye, Water Sci Eng 13 (2020) 286–298, https://doi.org/10.1016/j.wse.2020.12.001.

[8] R.J. Kadhim, F.H. Al-Ani, M. Al-Shaeli, Q.F. Alsalhy, A. Figoli, Removal of dyes using graphene oxide (Go) mixed matrix membranes, Membranes (Basel) 10 (2020) 1–24, https://doi.org/10.3390/membranes10120366.

[9] G. Vijayaraghavan, S. Shanthakumar, Removal of crystal violet dye in textile effluent by coagulation using algal alginate from brown algae sargassum sp, Desalination Water Treat 196 (2020) 402–408, https://doi.org/10.5004/dwt.2020.25569.

[10] A. Azari, R. Nabizadeh, A.H. Mahvi, S. Nasseri, Magnetic multi-walled carbon nanotubes-loaded alginate for treatment of industrial dye manufacturing effluent: adsorption modelling and process optimisation by central composite face-central design, Int J Environ Anal Chem 2 (2021) 1–21, https://doi.org/10.1080/03067319.2021.1877279.

[11] V. Katheresan, J. Kansedo, S.Y. Lau, Efficiency of various recent wastewater dye removal methods: a review, J Environ Chem Eng 6 (2018) 4676–4697, https://doi.org/10.1016/j.jece.2018.06.060.

[12] A. Azari, M. Yeganeh, M. Gholami, M. Salari, The superior adsorption capacity of 2,4-Dinitrophenol under ultrasound-assisted magnetic adsorption system: modeling and process optimization by central composite design, J Hazard Mater 418 (2021) 126348, https://doi.org/10.1016/j.jhazmat.2021.126348.

[13] H. Xiang, G. Ren, Y. Zhong, D. Xu, Z. Zhang, X. Wang, et al., Fe3 o4 @c nanoparticles synthesized by in situ solid-phase method for removal of methylene blue, Nanomaterials 11 (2021) 1–20, https://doi.org/10.3390/nano11020330.

[14] R. Li, Y. Gao, X. Jin, Z. Chen, M. Megharaj, R. Naidu, Fenton-like oxidation of 2,4-DCP in aqueous solution using iron-based nanoparticles as the heterogeneous catalyst, J Colloid Interface Sci 438 (2015) 87–93, https://doi.org/10.1016/j.jcis.2014.09.082.

[15] A. Alayli, H. Nadaroglu, E. Turgut, Nanobiocatalyst beds with Fenton process for removal of methylene blue, Appl Water Sci 11 (2021) 1–8, https://doi.org/10.1007/s13201-021-01367-8.
[16] B. Kakavandi, A. Takdastan, S. Pourfadakari, M. Ahmadmoazzam, S. Jorfi, Heterogeneous catalytic degradation of organic compounds using nanoscale zero-valent iron supported on kaolinite: mechanism, kinetic and feasibility studies, J Taiwan Inst Chem Eng 96 (2019) 329–340, https://doi.org/10.1016/j.jtice.2018.11.027.
[17] K. Li, Y. Zhao, C. Song, X. Guo, Magnetic ordered mesoporous Fe 3 O 4/CeO 2 composites with synergy of adsorption and Fenton catalysis, Appl Surf Sci 425 (2017) 526–534, https://doi.org/10.1016/j.apsusc.2017.07.041.
[18] G. Gopal, H. Sankar, C. Natarajan, A. Mukherjee, Tetracycline removal using green synthesized bimetallic nZVI-Cu and bentonite supported green nZVI-Cu nanocomposite: a comparative study, J Environ Manag 254 (2020) 109812, https://doi.org/10.1016/j.jenvman.2019.109812.
[19] S.R. Dhruval, N. Pai, S.S. Dhanwant, B. Hussein, S. Nayak, C.V. Rao, et al., Rapid synthesis of antimicrobial Fe/Cu alloy nanoparticles using Waste Silkworm Cocoon extract for cement mortar applications, Adv Nat Sci Nanosci Nanotechnol 11 (2020), 025006, https://doi.org/10.1088/2043-6254/ab8790.
[20] A. Galdames, L. Ruiz-Rubio, M. Orueta, M. Sánchez-Arzalluz, J.L. Vilas-Vilela, Zero-valent iron nanoparticles for soil and groundwater remediation, Int J Environ Res Publ Health 17 (2020) 1–23, https://doi.org/10.3390/ijerph17165817.
[21] Y. Rashtbari, S. Hazrati, A. Azari, S. Afshin, M. Fazlzadeh, M. Vosoughi, A novel, eco-friendly and green synthesis of PPAC-ZnO and PPAC-nZVI nanocomposite using pomegranate peel: cephalexin adsorption experiments, mechanisms, isotherms and kinetics, Adv Powder Technol 31 (2020) 1612–1623, https://doi.org/10.1016/j.apt.2020.02.001.
[22] H.M. Abd El-Aziz, R.S. Farag, S.A. Abdel-Gawad, Removal of contaminant metformin from water by using Ficus benjamina zero-valent iron/copper nanoparticles, Nanotechnol Environ Eng 5 (2020) 1–9, https://doi.org/10.1007/s41204-020-00086-w.
[23] H. Patel, Fixed-bed column adsorption study: a comprehensive review, Appl Water Sci 9 (2019) 1–17, https://doi.org/10.1007/s13201-019-0927-7.
[24] D. Charumathi, N. Das, Packed bed column studies for the removal of synthetic dyes from textile wastewater using immobilised dead C. tropicalis, Desalination 285 (2012) 22–30, https://doi.org/10.1016/j.desal.2011.09.023.
[25] Y. Süzen, C. Ozmetin, Removal of reactive black 5 dye using fenton oxidation from aqueous solutions and optimization of response surface methodology, Desalination Water Treat 172 (2019) 106–114, https://doi.org/10.5004/dwt.2019.24943.
[26] R. Venkataraghavan, R. Thiruchelvi, D. Sharmila, Statistical optimization of textile dye effluent adsorption by Gracilaria edulis using Plackett-Burman design and response surface methodology, Heliyon 6 (2020), e05219, https://doi.org/10.1016/j.heliyon.2020.e05219.
[27] H.M. Abdel-Aziz, R.S. Farag, S.A. Abdel-Gawad, Carbamazepine removal from aqueous solution by green synthesis zero-valent iron/Cu nanoparticles with Ficus benjamina leaves' extract, Int J Environ Res 13 (2019) 843–852, https://doi.org/10.1007/s41742-019-00220-w.
[28] S.M. Alardhi, T.M. Albayati, J.M. Alrubaye, Adsorption of the methyl green dye pollutant from aqueous solution using mesoporous materials MCM-41 in a fixed-bed column, Heliyon 6 (2020), e03253, https://doi.org/10.1016/j.heliyon.2020.e03253.
[29] M.T. Yagub, T.K. Sen, S. Afroze, H.M. Ang, Fixed-bed dynamic column adsorption study of methylene blue (MB) onto pine cone, Desalination Water Treat 55 (2015) 1026–1039, https://doi.org/10.1080/19443994.2014.924034.
[30] S.S. Madan, B.S. De, K.L. Wasewar, Adsorption performance of packed bed column for benzylformic acid removal using CaO2 nanoparticles, Chem Data Collect 23 (2019) 1–16, https://doi.org/10.1016/j.cdc.2019.100267.
[31] L. Shaker Ardakani, V. Alimardani, A.M. Tamaddon, A.M. Amani, S. Taghizadeh, Green synthesis of iron-based nanoparticles using Chlorophytum comosum leaf extract: methyl orange dye degradation and antimicrobial properties, Heliyon 7 (2021), e06159, https://doi.org/10.1016/j.heliyon.2021.e06159.
[32] K.M. Al-Qahtani, Cadmium removal from aqueous solution by green synthesis zero valent silver nanoparticles with Benjamina leaves extract, Egypt, J Aquat Res 43 (2017) 269–274, https://doi.org/10.1016/j.ejar.2017.10.003.
[33] E.A. Mohamed, Green synthesis of copper & copper oxide nanoparticles using the extract of seedless dates, Heliyon 6 (2020), e03123, https://doi.org/10.1016/j.heliyon.2019.e03123.
[34] Z. Elahimehr, F. Nemati, A. Elhampour, Synthesis of a magnetic-based yolk-shell nano-reactor: a new class of monofunctional catalyst by Cu0-nanoparticles and its application as a highly effective and green catalyst for A3 coupling reaction, Arab J Chem 13 (2020) 3372–3382, https://doi.org/10.1016/j.arabjc.2018.11.011.
[35] M. Khashij, A. Dalvand, M. Mehralian, A.A. Ebrahimi, R. Khosravi, Removal of reactive black 5 dye using zero valent iron nanoparticles produced by a novel green synthesis method, Pigment Resin Technol 49 (2020) 215–221, https://doi.org/10.1108/PRT-10-2019-0092.
[36] M. Nasrollahzadeh, S.M. Sajadi, M. Khalaj, Green synthesis of copper nanoparticles using aqueous extract of the leaves of Euphorbia esula L and their catalytic activity for ligand-free Ullmann-coupling reaction and reduction of 4-nitrophenol, RSC Adv 4 (2014) 47313–47318, https://doi.org/10.1039/c4ra08863h.
[37] A.R. Puthukkara P, S. Jose T, D. lal S, Plant mediated synthesis of zero valent iron nanoparticles and its application in water treatment, J Environ Chem Eng 9 (2021) 1–77, https://doi.org/10.1016/j.jece.2020.104569.
[38] S. Hashemian, Fenton-like oxidation of malachite green solutions: kinetic and thermodynamic study, J Chem 2013 (2013) 1–7, https://doi.org/10.1155/2013/809318.
[39] X. Wei, X. Xie, Y. Wang, S. Yang, Shape-dependent fenton-like catalytic activity of Fe3O4 nanoparticles, J Environ Eng 146 (2020), 04020005, https://doi.org/10.1061/(asce)ee.1943-7870.0001648.
[40] N.A. Youssef, S.A. Shaban, F.A. Ibrahim, A.S. Mahmoud, Degradation of methyl orange using Fenton catalytic reaction, Egypt, J Petrol 25 (2016) 317–321, https://doi.org/10.1016/j.ejpe.2015.07.017.
[41] A.R.A. Giwa, I.A. Bello, A.B. Olabintan, O.S. Bello, T.A. Saleh, Kinetic and thermodynamic studies of fenton oxidative decolorization of methylene blue, Heliyon 6 (2020), e04454, https://doi.org/10.1016/j.heliyon.2020.e04454.
[42] J.H. Park, J.J. Wang, R. Xiao, N. Tafti, R.D. DeLaune, D.C. Seo, Degradation of Orange G by Fenton-like reaction with Fe-impregnated biochar catalyst, Bioresour Technol 249 (2018) 368–376, https://doi.org/10.1016/j.biortech.2017.10.030.
[43] B. Yang, Z. Tian, L. Zhang, Y. Guo, S. Yan, Enhanced heterogeneous Fenton degradation of Methylene Blue by nanoscale zero valent iron (nZVI) assembled on magnetic Fe3O4/reduced graphene oxide, J Water Proc Eng 5 (2015) 101–111, https://doi.org/10.1016/j.jwpe.2015.01.006.
[44] S. Sadaf, H.N. Bhatti, M. Arif, M. Amin, F. Nazar, M. Sultan, Box–Behnken design optimization for the removal of Direct Violet 51 dye from aqueous solution using lignocellulosic waste, Desalination Water Treat 56 (2015) 2425–2437, https://doi.org/10.1080/19443994.2014.968215.
[45] M. Cai, J. Su, Y. Zhu, X. Wei, M. Jin, H. Zhang, et al., Decolorization of azo dyes Orange G using hydrodynamic cavitation coupled with heterogeneous Fenton process, Ultrason Sonochem 28 (2016) 302–310, https://doi.org/10.1016/j.ultsonch.2015.08.001.
[46] M.H. Marzbali, M. Esmaieli, Fixed bed adsorption of tetracycline on a mesoporous activated carbon: experimental

study and neuro-fuzzy modeling, J Appl Res Technol 15 (2017) 454–463, https://doi.org/10.1016/j.jart.2017.05.003.

[47] F. Emami, A.R. Tehrani-Bagha, K. Gharanjig, F.M. Menger, Kinetic study of the factors controlling Fenton-promoted destruction of a non-biodegradable dye, Desalination 257 (2010) 124–128, https://doi.org/10.1016/j.desal.2010.02.035.

[48] M. Ergüt, A. Özer, Heterogeneous Fenton-like decolorization of Procion Red MX-5B with iron-alginate gel beads as an effective catalyst, Teh Glas 13 (2019) 297–304, https://doi.org/10.31803/tg-20180201002727.

[49] J. Liu, G. Peng, X. Jing, Z. Yi, Treatment of methyl orange by the catalytic wet peroxide oxidation process in batch and continuous fixed bed reactors using Fe-impregnated 13X as catalyst, Water Sci Technol 78 (2018) 936–946, https://doi.org/10.2166/wst.2018.372.

[50] S. Punathil, D. Ghime, T. Mohapatra, C. Thakur, P. Ghosh, Fixed bed reactor for removal of methylene blue dye using heterogeneous fenton catalyst, J Hazardous Toxic Radioact Waste 24 (2020), 04020037, https://doi.org/10.1061/(asce)hz.2153-5515.0000534.

[51] F.S. De Oliveira Cruz, M.A. Nascimento, G.A. Puiatti, A.F. De Oliveira, A.H. Mounteer, R.P. Lopes, Textile effluent treatment using a fixed bed reactor using bimetallic Fe/Ni nanoparticles supported on chitosan spheres, J Environ Chem Eng 8 (2020) 1–9, https://doi.org/10.1016/j.jece.2020.104133.